ELSEVIER

Atmospheric Research 45 (1997) 81–107

ATMOSPHERIC RESEARCH

Testing the effect of a two-way-coupling of a meteorological and a hydrologic model on the predicted local weather

Nicole Mölders *, Armin Raabe

LIM, Institut für Meteorologie, Universität Leipzig, Stephanstraße 3, Leipzig D-04103, Germany

Received 10 March 1997; received in revised form 24 June 1997; accepted 24 June 1997

Abstract

A land-surface module to couple a meteorological and a hydrologic model was developed to simulate the water cycle in a closed manner. The module allows to consider the hydrologic processes of the river catchment (translation, retention, lateral discharge) in the meteorological model which itself drives the hydrologic model by predicted evapotranspiration and precipitation. Besides this two-way-coupling, the module allows to consider subgrid-scale surface processes and to heterogenize precipitation in the meteorological model. The results of 24-h simulations with and without a two-way-coupling of the models substantiate that even on a short time scale surface runoff and lateral water flows affect soil wetness, soil temperature, cloudiness and the thermal regime of the atmospheric boundary layer within the catchment. As expected, the coupling results in a slight trend towards moister valleys and drier hills. © 1997 Elsevier Science B.V.

1. Introduction

The water cycle is a major part of the global climate system. Over land, its major components include precipitation, groundwater, evapotranspiration, ice and snowmelt, as well as river runoff (Kuhl and Miller, 1992). Although, at any given time, rivers hold only a fraction of the world's total water, they provide the critical link for returning water from continents to the ocean (Miller et al., 1994). For individual river catchments, runoff depends on precipitation and evapotranspiration within the basin and the ability

* Corresponding author.

PII S0169-8095(97)00035-5

of the land to store water (Liston et al., 1994). Water storage within the river basins among others depends on soil type, soil depth, surface heterogeneity and vegetation cycle (Miller et al., 1994).

As a first approximation, meteorological models usually neglect lateral flows of soil water (e.g., Pielke, 1984), surface runoff, the transport of water by river flow as well as the re- and discharge of the groundwater storage. This means that they do not simulate a closed water cycle. Nevertheless, these surface and sub-surface hydrologic processes may be of great relevance in climate modeling as well as in weather forecasting. In GCMs, for instance, river runoff is an important input value for ocean models as freshwater flow affects the thermohaline circulation of the ocean. In weather forecast models, for example, the neglecting of lateral soil water movements and surface runoff may yield to an underestimation of soil moisture in river valleys and an overestimation of soil moisture in the nearby mountainous regions which usually receive more precipitation (e.g., Müller et al., 1995).

Such wrong distributions of dry and wet surfaces, however, may significantly affect the local water supply to the atmosphere (e.g., Milly and Dunne, 1994) and, hence, modeled cloud and precipitation formation, as well as the quality of numerical weather prediction (e.g., Müller et al., 1995).

To more appropriately model the water cycle, hydrologic and meteorological concepts have to be matched. Recently, several authors (e.g., Kuhl and Miller, 1992; Marengo et al., 1994; Miller et al., 1994; Sausen et al., 1994; Hagemann and Dümenil, 1996) suggested parameterizations of different complexity to directly parameterize runoff in GCMs. In an attempt to model global runoff, Kuhl and Miller (1992) suggested a simple scheme wherein all runoff within a river drainage basin instantaneously reaches the river mouth. Although the global runoff agreed well with the observed runoff locally large errors occurred. In 1994, Sausen et al. proposed a one-parameter model that represented each grid cell by a two-dimensional linear reservoir with different retention coefficients for the flows in four directions (east, west, north, south). Herein, these coefficients depend on the orography and grid size. This approach, however, does not distinguish the different types of flow processes. The river model introduced by Miller et al. (1994) allows the excess water at the surface calculated by a GCM to run off into the river within a continental grid cell. The direction and speed of flow is either constant or depends on topography gradient. More recently, in an attempt to improve Sausen et al.'s approach, Hagemann and Dümenil (1996) developed a global parameterization for ECHAM4-T42 using grid cell characteristics. Herein, equal linear reservoirs of the cascade for overland flow and river flow and a one-parameter model for baseflow are considered. The corresponding retention coefficients depend on topography gradient between two grid cells and on the grid size.

Another way to model more appropriately the water cycle is to directly couple a hydrologic and a meteorological model in a two-way manner. Herein, the hydrologic processes of the river catchment are considered in the atmospheric model, which itself drives the hydrologic model. This means that the precipitation and the evapotranspiration predicted by the meteorological model serve as input for the hydrologic model, while the runoff and the lateral water flows determined by the hydrologic model are considered in the calculation of soil wetness by the meteorological model.

In this paper, such a two-way-coupling of a meso-β-scale meteorological model with a runoff model is described and tested for the short time scale, usually considered by such type of meteorological models. In the discussion, the main focus is on the impact of the two-way-coupling on the predicted soil wetness and the atmospheric water cycle.

2. Brief description of the models

2.1. The meteorological model

The Leipzig's version of the non-hydrostatic model GESIMA (**GE**esthacht's **SI**mulation **M**odel of the **A**tmosphere; e.g., Kapitza and Eppel, 1992; Eppel et al., 1995) is used in this study. Its dynamical part bases on the anelastic equations.

Radiation transfer is calculated by a simple bulk-formula. A five water class (water vapor, cloud water, rainwater, ice, graupel) bulk-parameterization of cloud microphysics is applied (Mölders et al., 1997). It considers the condensation of water vapor, the evaporation of cloud water and rainwater, the formation of rainwater by melting of ice and graupel, autoconversion and coalescence. Moreover, the riming of supercooled cloud water onto ice crystals and graupel, the freezing of rain drops to graupel and of cloud water to ice, the sublimation of ice and graupel, the deposition of water vapor onto ice and graupel, the conversion from ice crystals to graupel as well as the sedimentation of rainwater, ice, and graupel are taken into account.

The parameterization of the soil–vegetation–atmosphere interaction follows Deardorff (1978) (see also Eppel et al., 1995) assuming homogeneous landuse characteristics. The surface stress and the near-surface fluxes of heat and water vapor are expressed in terms of dimensionless drag and transfer coefficients using the parametric model of Kramm et al. (1995) which is based on Monin–Obukhov similarity theory. Above the atmospheric surface layer, the turbulent fluxes of momentum are calculated by a one-and-a-half-order closure scheme. Here, the elements of the eddy diffusivity tensor are expressed by the vertical and the horizontal eddy diffusivities, which are related to the budget of turbulent kinetic energy (TKE) and the mixing length using the Kolmogorov–Prandtl relationship (see also Kapitza and Eppel, 1992).

2.2. The hydrologic model

The hydrologic model NASMO (**N**iederschlag–**A**bfluß–**S**imulations–**MO**dell, i.e., precipitation runoff model; Maniak, 1996) is a conceptual physically based model. It assumes that the total rainfall volume is allocated to (1) initial abstraction which is the amount of storage that must be satisfied before event flow can start, (2) retention of water (after the end of the initial abstraction), which does not contribute to the event flow, and (3) event flow (Maniak, 1996). Initial abstraction consists of interception, evaporation, and filling of hollows.

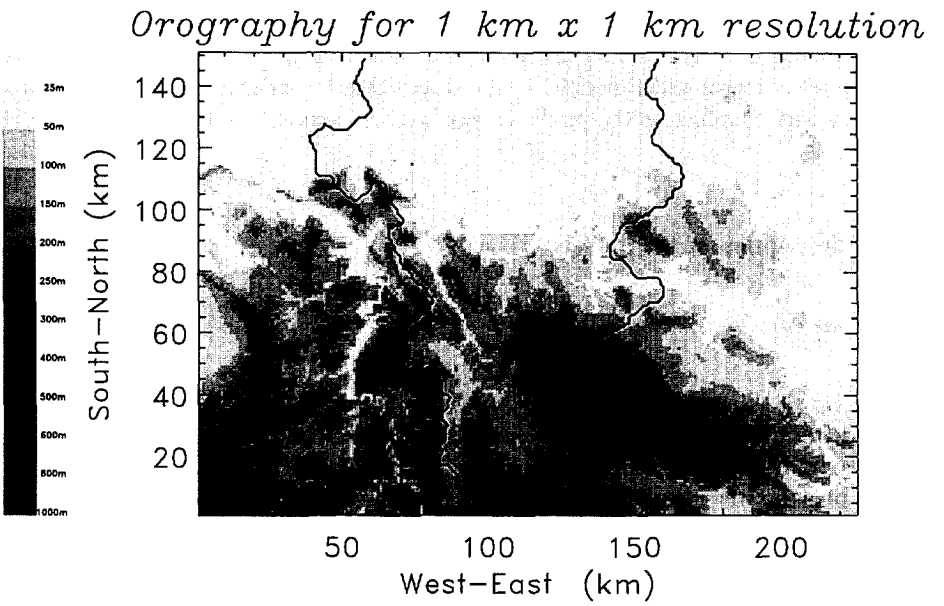

Fig. 1. Topography in 1×1 km^2 resolution. The domain of the hydrologic model is superimposed by thick lines. White areas stand for elevations lower than 25 m.

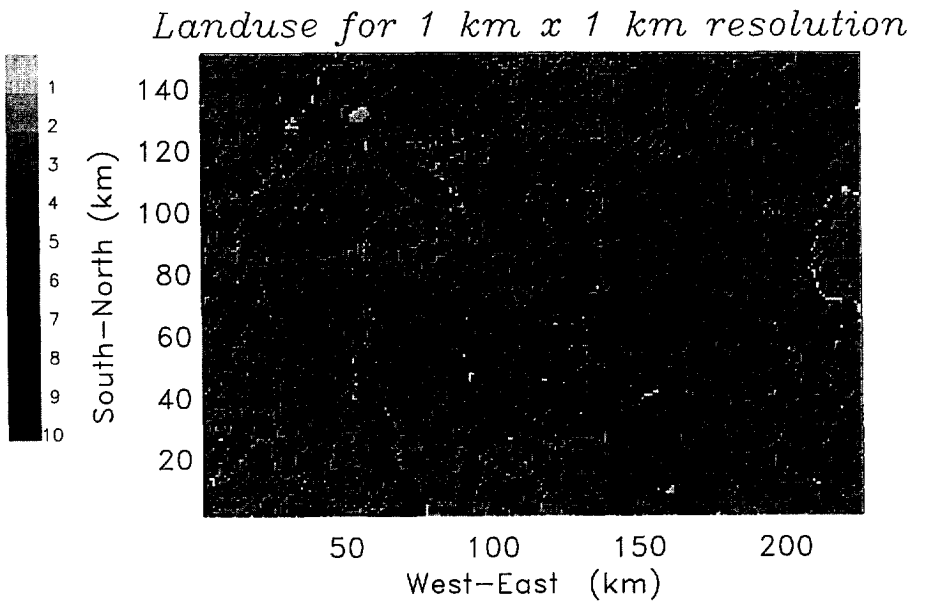

Fig. 2. Landuse in 1×1 km^2 resolution. The landuse types are denoted as 1 *water*, 2 *sand*, 3 *grassland*, 4 *agriculture*, 5 *heather / bushland*, 6 *deciduous forest*, 7 *mixed forest*, 8 *coniferous forest*, 9 *settlements*, and 10 *city*, respectively.

The model distinguishes between surface runoff, subsurface flow, and groundwater flow. Storage capacity depends on soil type and landuse as well as on the temporal evolution of precipitation in the hours before. Six runoff relevant classes are distinguished. Water may flow in eight directions (depending on topography gradient), namely, into the neighbored grid cells and into those at the four corners of a grid cell (Maniak, 1996).

2.3. Model domains

Since hydrologic models are bounded to drainage basins, the model domains of NASMO and GESIMA are not the same (see, e.g., Fig. 1. Hence, NASMO only considers the southern part of the Aller catchment for which a lot of the rivers of its sub-basins start in the Harz, a mountainous region in Mid-Germany. The horizontal resolution of the grid is 1×1 km^2.

The meteorological model encompasses a 225 km $\times$ 150 km region around the Harz (Figs. 1 and 2). The vertical resolution varies from 20 m close to the ground to 1 km at the top of the model with 8 levels below 2 km and 10 above that height. The horizontal resolution of the atmospheric grid cells is 5×5 km^2.

3. Computational procedures

Obviously, the temporal and the spatial scales considered in hydrologic models allow much longer time steps but require much finer model grid resolutions than those regarded in meteorological models. Unfortunately, in meteorological models, a better representation of the surface characteristics may not be achieved by a finer grid resolution due to (1) parameterization limitations, the limited availability of (2) initial data (e.g., soil wetness) and of (3) computer resources. The latter problem will hopefully be overcome with the next generation of parallel computers. The first point, however, will require strong efforts on model development and has to be addressed within the next future to be able to take advantage of the increasing computer capacity of the next generation of computers. Such limitations of parameterizations are the scale dependency of some assumptions and threshold values. The parameterization of the drag and transfer coefficients, for instance, which bases on Monin–Obukhov theory, was derived for a fetch to horizontal extension ratio of 1:100. Hence, for a reference height of 10 m as used in the presented model configuration, this theory may not be applied for grid resolutions smaller than 1 km (e.g., Mahrt and Sun, 1995; Tetzlaff and Mölders, 1997). Another example is the threshold value for autoconversion which depends on the grid resolution (see, e.g., Kessler, 1969; Mölders et al., 1995). The limited availability of initial data is a more serious problem. As an example, several sensitivity studies were performed using different soil wetness values to test the impact of the initial soil wetness on predicted cloud and precipitation formation. It was found that the greatest differences in predicted cloud extension, precipitation pattern and intensity will occur if the initial soil wetness values are between 0.2 and 0.7 m^3 m^{-3}. For values greater than these, the predicted distributions hardly differ among each other. Similar is true for initial values of soil wetness lower than 0.2 m^3 m^{-3}.

Hence, as a consequence of the aforementioned limitations on one hand parameterizations to downscale the hydrologically relevant quantities provided by meteorological models are required to utilize evapotranspiration and precipitation as input to a hydrologic model. On the other hand, aggregation procedures are needed to upscale those quantities, which are of relevance for the hydrologic model to deliver differences of lateral water flow for use in the determination of soil wetness in the meteorological model.

3.1. Downscaling of precipitation, evapotranspiration and soil wetness

In the meteorological model, an explicit subgrid-scheme, suggested by Seth et al. (1994) for the global scale, is adapted for the meso-β-scale to downscale the hydrologically relevant quantities (Mölders et al., 1996). Herein, a higher resolution grid (1×1 km^2) consisting of N ($= 25$ in our study) subgrid cells per grid cell (5×5 km^2) is defined (Fig. 3). These subgrid cells are considered to be homogeneously covered by their dominant vegetation and soil types (Fig. 2). Unique energy and hydrologic budgets (Eqs. (1)–(4), (7) and (8)) are maintained for each subgrid cell using the subgrid cell forcing at the representative location, i.e., in each subgrid cell, the fluxes are individually calculated with their own subgrid soil temperatures, soil wetness and near-surface

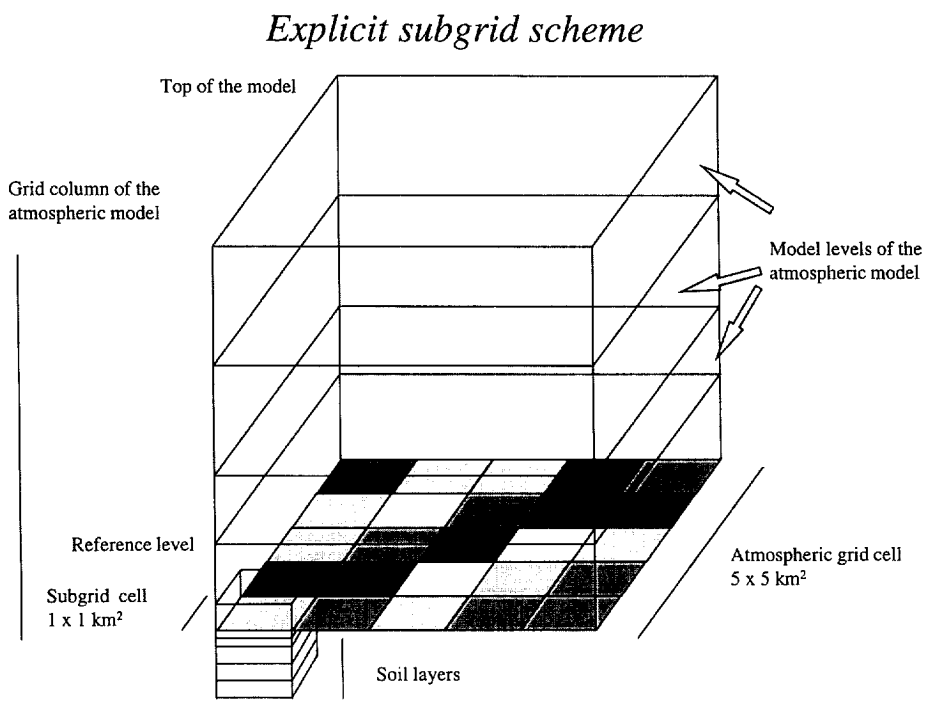

Fig. 3. Schematic view of a grid column and its subgrid cells within the meteorological model (modified after Mölders et al., 1996). Areas of different grey level represent different landuse types.

meteorological forcing in the immediate vicinity of the Earth's surface. Soil wetness, soil temperature as well as near surface air temperature and moisture are stored for each subgrid cell and serve to determine these quantities in the next time step. The net radiation, Q, the soil heat flux, G, the fluxes of sensible, H, and latent heat, $L_v E$, of the mth subgrid cell of the jth grid cell are, therefore, given by (Mölders et al., 1996)

$$Q_{m,j} = -S_{m,j}(1-\alpha_{m,j}) - \varepsilon_{m,j} L_{m,j} + \varepsilon_{m,j}\sigma T_{gm,j}^4, \tag{1}$$

$$G_{m,j} = \begin{cases} -\lambda_{m,j}\partial T_{gm,j}/\partial z, & \text{for land} \\ Q_{m,j} + L_v E_{m,j} + H_{m,j}, & \text{for water} \end{cases} \tag{2}$$

$$H_{m,j} = \rho c_p C_{hm,j} u_{rj}(\Theta_{gm,j} - \Theta_{rj}), \tag{3}$$

$$L_v E_{m,j} = \begin{cases} \rho L_v C_{qm,j} u_{rj}(q_{sm,j}(T_{fm,j}) - q_{rj}) w_{em,j}, & \text{for vegetation} \\ \rho L_v C_{qm,j} u_{rj}(q_{sm,j}(T_{gm,j}) - q_{rj}) w_{em,j}, & \text{elsewise} \end{cases} \tag{4}$$

where the subscripts g, f, and r stand for the ground, the foliage surface, and the reference height located at the first half level in 10 m height above ground. A list of the parameters used in the equations is given in Appendix A. For bare soil, the so-called wetness factor (e.g., Deardorff, 1978),

$$w_{em,j} = \begin{cases} f_{m,j}, & \text{for bare soil} \\ 1, & \text{for water} \\ g_{sm,j}/(g_{sm,j} + C_{qm,j} u_{rj}), & \text{for vegetation} \end{cases} \tag{5}$$

equals the soil wetness factor, f, while for vegetated surfaces it considers canopy conductivity, g_s, which depends on the maximal evaporative conductivity, g_1 (Table 1), insolation, water vapor deficit, air temperature and soil wetness. Soil wetness depends on evapotranspiration and precipitation, transport from the ground water to the surface and, in a two-way-coupled simulation, also from the differences of lateral inflow and outflow of the subgrid cells (see Eq. (8) in Section 3.3).

Table 1
Parameters as used for the different landuse types (from Wilson et al., 1987 and Eppel et al., 1995). The quantities indicated by * are calculated by the model

Landuse type	k_s	c_i	ε	α	z_0	w_k	α_c	g_1
	10^{-6} m^2 s^{-1}	10^6 J m^{-3} K^{-1}			m	m	10^{-3} kg m^{-3} s^{-1}	m s^{-1}
Water	0.15	4.2	0.94	*	*	1.0	1000	–
Sand	0.84	2.1	0.90	0.3	0.0004	0.002	0.9	–
Grassland	0.56	2.1	0.95	0.25	0.02	0.010	8.0	0.04
Agriculture	0.74	2.9	0.95	0.18	0.04	0.005	3.0	0.04
Heather / Bushland	0.70	2.5	0.95	0.15	0.35	0.003	1.0	0.024
Decidous forest	0.70	2.5	0.97	0.20	0.8	0.010	8.0	0.023
Mixed forest	0.70	2.5	0.95	0.175	0.9	0.010	8.0	0.023
Coniferous forest	0.70	2.5	0.98	0.15	1.0	0.010	8.0	0.023
Settlements	1.0	2.0	0.90	0.20	0.8	0.003	1.0	–
City	1.0	2.0	0.95	0.15	1.0	0.002	0.9	–

The coupling to the jth atmospheric grid cell is realized by arithmetically averaging the individual subgrid cell fluxes, $F^k_{m,j}$, to provide the grid cell fluxes

$$F^k_j = \frac{1}{N} \sum_{m=1}^{N} F^k_{m,j}, \tag{6}$$

where the index k stands for the fluxes ($L_v E$, H, G, Q).

All water enters the land phase of the hydrologic cycle as precipitation. Thus, to assess, predict and forecast hydrologic responses, it is required to understand how the amount, rate and duration of precipitation are distributed in time and space (Dingman, 1994). Unfortunately, precipitation variability over complex terrain is difficult to predict, especially at small spatial scales, such as over a small watershed. Such variability can be critically important for accurately determining the water budget of a region (Johnson and Hanson, 1995). Recently, statistically and physically based modeling approaches to estimate mountainous precipitation have been developed. Especially, for GCMs recent work aimed at better determining regional precipitation through nesting limited-area models (e.g., Giorgi, 1990) or through downscaling (e.g., von Storch et al., 1993; Leung and Ghan, 1995). In most regions of the world, long-lasting precipitation increases with elevation (orographic effect) because horizontally moving air encounters a topographic barrier and, hence, acquires vertical motion when passing the barrier. The related cooling leads to precipitation. In Mid-Europe, the annual precipitation increases on average 50 mm per 100 m terrain elevation, where this gradient is stronger for maritime than for continental conditions (Pleiss, 1977). According to these findings in this case study, precipitation is heterogenized by relating precipitation to surface elevation (Mölders et al., 1996)

$$P_{m,j} = \left(z_{m,j}/z_j\right) P_j. \tag{7}$$

Here, z_j and $z_{m,j}$ are the mean terrain height of the jth grid cell and the mth subgrid cell and P_j is the mean precipitation predicted for the jth grid cell by the cloud module. Eq. (7) means that subgrid cells elevated higher than the mean terrain height of the atmospheric grid cell receive more precipitation than those subgrid cells which are located lower than that height. Note that Eq. (7) does not consider that there might be fractions of the grid cell which do not receive precipitation at all, i.e., it is not suitable for convective precipitation events.

Obviously, the explicit subgrid scheme ignores subgrid-scale dynamical effects related to the surface heterogeneity, for instance, directed flows caused by topography effects. Moreover, it also neglects advective effects accompanied by occasionally observed internal boundary layers (e.g., Raabe, 1983, 1991; Hupfer and Raabe, 1994) and interaction between the energy budgets of the different landuse types.

3.2. Upscaling of runoff

As already mentioned, the assumptions made on the parameterizations of the drag and transfer coefficients are scale-dependent (Mahrt and Sun, 1995), for which the explicit subgrid scheme should not be applied at scales much smaller than 1×1 km^2. NASMO and GESIMA apply the same landuse distribution as shown in Fig. 2. This means that the runoff behavior of a subgrid cell may not vary by vegetation effects. Due

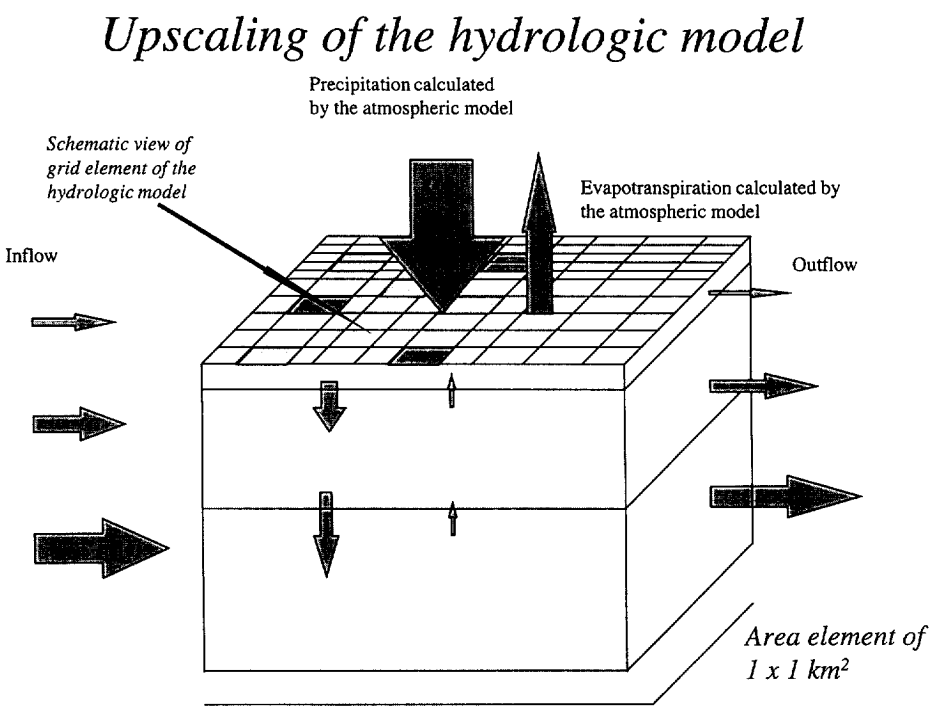

Fig. 4. Schematic view of the upscaling procedure applied in NASMO (modified after Maniak, 1996). Areas of different grey level represent different hydrologic characteristics (e.g., slope, direction of flow, flow length, etc.).

to the irregularity of the terrain, for instance, the hydrologic characteristics (e.g., flow direction, flow length, retention, initial abstraction, etc.) may significantly vary within 1×1 km^2. Therefore, they are considered on a 100-m grid resolution. These grid cells of 100 m side length are superposed to 1×1 km^2 areas (Fig. 4), which correspond to GESIMA's subgrid cells, by forming area weighted means (e.g., Kleeberg and Øverland, 1989; Maniak, 1996). Then the runoff, lateral flows, and ground water flows are calculated for the respective GESIMA subgrid cell on a 1×1 km^2 resolution using the effective precipitation delivered by GESIMA and the area weighted hydrological properties (Beckmann, Th., 1997, private communication).

Note that a comparison of the runoff predicted by a stand-alone version of NASMO, which used observed precipitation data, with observed runoff showed that in most of the cases the aggregation described above provides good results. It usually delivers better results than to calculate the water flows on the finer grid and to determine the area-weighted flows from these values afterwards (e.g., Kleeberg and Øverland, 1989; Beckmann, Th., 1997, private communication).

3.3. Two-way-coupling

In nature, the coupling of the atmospheric and the land phase of the water cycle occurs through mass (precipitation and evapotranspiration) and energy exchanges. In a

first step, the influence of soil temperature on soil wetness is neglected in the coupling of GESIMA and NASMO to avoid additional degrees of freedom. This means that the coupling bases on mass conservation only. Herein, a balance between the sources of water by precipitation, groundwater discharge and lateral inflow, the sinks of water by lateral outflow, groundwater recharge, and evapo(transpi)ration are conceptually balanced with the change in soil wetness (Eq. (8)).

Differences of lateral in- and outflow within a 1×1 km^2 area are provided by NASMO (e.g., Fig. 5) for each GESIMA subgrid cell in an hourly sequence because NASMO runs with a time step of 1 h. GESIMA, however, uses a time step of 20 s (to satisfy the Courant-criterion). Therefore, the differences of lateral in- and outflow are assumed to be constant in time for one hour duration to determine the difference in lateral flow per GESIMA time step for use in the third term of Eq. (8). Thus, distributing the lateral difference onto the hour allows to consider the contribution of the lateral

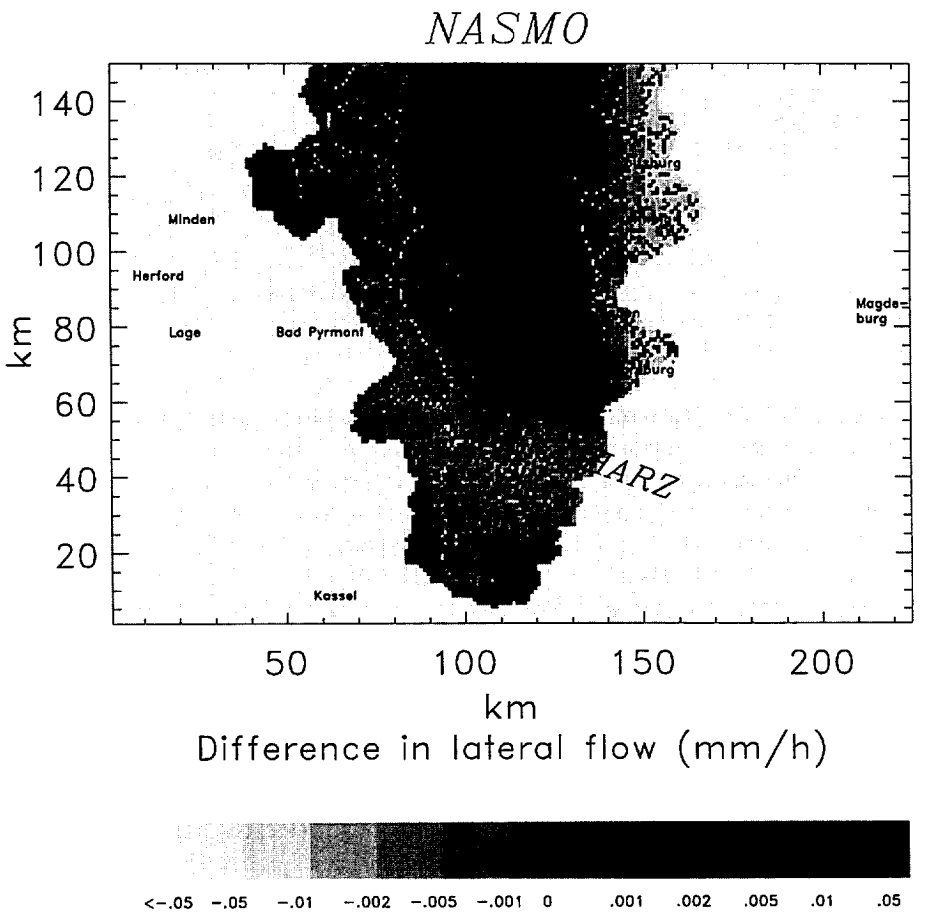

Fig. 5. Differences of lateral flow (mm h^{-1}) as determined by NASMO for 24 LT (data from Beckmann, Th., 1997, private communication). White areas within the catchment stand for lateral flow differences lower than -0.05 mm h^{-1}.

flows in each GESIMA time step. In the hourly sum, of course, the same lateral change is achieved.

Sensitivity studies were performed which considered the (total) hourly change of the differences in lateral in- and outflow once per hour, i.e., only at the full hour the differences provided by NASMO serve as input while at the other time steps the third term of Eq. (8) is zero. It was found that such an exchange of the data lead to an unrealistic (stepwise) behavior of the temporal change of soil wetness. Therefore, such a method of coupling was rejected.

Hence, in the jth grid cell, the change of the soil wetness of the mth subgrid cell of GESIMA is given by

$$\frac{\partial f_{m,j}}{\partial t} = \frac{E_{m,j} - P_{m,j}}{w_{\mathrm{k}m,j}\rho_{\mathrm{w}}} + \frac{\alpha_{\mathrm{c}m,j}}{\rho_{\mathrm{w}}}\left(1 - f_{m,j}\right) + \beta_{m,j}\frac{R_{m,j}}{w_{\mathrm{k}m,j}\rho_{\mathrm{w}}}, \tag{8}$$

where ρ_{w} is the density of water, and R is the difference between the lateral in- and outflow, respectively. Further, w_{k} represents the amount of water that a soil layer may uptake before saturation occurs and α_{c} is the capillarity. The parameter β serves to apply the original formulation of the soil wetness calculation of GESIMA in those regions where NASMO and GESIMA do not overlap (Fig. 1). It is equal to 1 in the catchment area and zero elsewhere. Note that β will also be zero if only GESIMA drives NASMO without re-coupling (one-way coupling) or if GESIMA runs alone.

The first term on the right hand side of Eq. (8) represents the external forcing by evapotranspiration and precipitation. The second term stands for the transport of water from the ground water to the surface, and the third term delivers the contribution of the river catchment.

It has to be pointed out that river flow is not explicitly taken into account and that all excess water (with respect to the saturation of the soil) is absorbed, exported and/or evapo(transpi)rated within the subgrid cells. That means NASMO predicts only the supply for runoff within the 1×1 km^2 areas. However, river flow should decrease the water availability within a subgrid cell because it continuously passes the cell borders. Thus, the simplification of hydrology accepted in the coupling described here may result in higher latent heat fluxes than in the case when river flow is considered. This artifact is due to the fact that on a 1×1 km^2 resolution of GESIMA's subgrid cells and even on the 100×100 m^2 resolution of the NASMO cells the rivers of the basin are of subgrid-scale.

3.4. Technical data

At the moment, the procedure to run GESIMA and NASMO in a two-way-coupling mode requires still a lot of man-power because up to now the models run at Leipzig on a Convex 240 or a C3800 and at Braunschweig on a Sun-workstation, respectively. The data still have to be updated hourly via ftp and transformed to the respective model grids. Here, still a lot of work is to be done to automatically run the model package GESIMA–NASMO. The CPU-time needed for one hour of simulation with GESIMA depends on the vertical and horizontal grid resolution, the resolution of the subgrid as well as on the number of grid points where cloud processes have to be calculated. In our case study, average 15 000 CPU-s are required for one hour of simulation time on the

C3800. NASMO runs about 120 CPU-s for one hour of simulation (Beckmann, Th., 1997, private communication).

4. Outline of the simulations

4.1. Initialization

Great effects on soil water may be expected for floodings. In Mid-Germany, flooding is often caused by large precipitation events in winter or spring. Since the impact of the solar forcing on the atmospheric water cycle is more strongly in spring than in winter, each atmospheric grid column of GESIMA was initialized using the profiles and conditions typical for floodings in early spring time (Table 2). Soil wetness was initialized as equal to 0.7 m^3 m^{-3} for all land subgrid cells. As pointed out in Section 3, this value is the lower limit of the insensitive range for greater values of soil wetness factors, which have to be expected for flooding events. Only in subgrid cells covered by water wetness is set equal to 1.

NASMO was initialized by a 48-h pre-run using precipitation data typically for flooding events. This pre-run is required by NASMO to avoid that the simulation time of interest starts with empty storages. Zero storage would mean that no runoff would occur during the simulation time because most of the precipitation would contribute to initial abstraction. Note that the coupled and the uncoupled simulation start with the same storage values.

Since GESIMA starts with zero cloud water, rainwater, ice and graupel, some spin up time is needed by GESIMA to develop the cloud and precipitation particles. Therefore, in the first six hours of our testing period, the models were run in a one-way mode to allow the meteorological model to spin up and to avoid that the soil wetness of the meteorological model will start to swing. Note that sensitivity studies, wherein the cloud and precipitating particles were initialized with those obtained by a simulation of the day

Table 2
Initial conditions

Height (m)	10	40	145	350	600	875	1250	1750	2500
Temperature (K)	282.4	282.2	281.2	279.6	277.4	275.2	274.0	273.8	269.2
Humidity (g kg^{-1})	5.040	5.040	5.037	5.020	4.971	4.756	4.909	4.784	3.742
Height (m)	3500	4500	5500	6500	7500	8500	9500	10500	11500
Temperature (K)	261.8	256.8	251.6	246.3	238.1	235.0	229.5	226.8	226.8
Humidity (g kg^{-1})	2.580	1.803	1.312	0.871	0.359	0.280	0.138	0.058	0.040

Geostrophic wind speed and direction: 10 m s^{-1} from 8°.
Pressure: 1006.8 h Pa.
Water surface temperature: 10°C.
Soil temperature at 1 m depth: 6.7°C.
Initial soil moisture: 0.7 m^3 m^{-3}.
Latitude: 51°N.
Julian day: 103.
Start time: 0000 LT.

before, showed that such an initialization does not improve the meteorological prediction. One-way mode means that GESIMA only drives NASMO but NASMO does not provide data to GESIMA. After the spin up time, the models run in a two-way-coupled mode.

4.2. Experimental design

If land evapotranspiration partially feeds precipitating clouds, then the land hydrology may influence its own forcing. Simulations with and without a two-way-coupling were performed to examine the impact of surface runoff and lateral flows on the hydrologically relevant quantities predicted by GESIMA. These runs are addressed, hereafter, as GWN (GESIMA coupled with NASMO) and REF (reference run), respectively.

The simulation results primarily differ in soil wetness (e.g., Figs. 6 and 7) due to the inclusion of surface runoff and lateral flows in GWN. This affects soil heat flux, soil temperature as well as surface temperature. The local decrease/increase of soil moisture

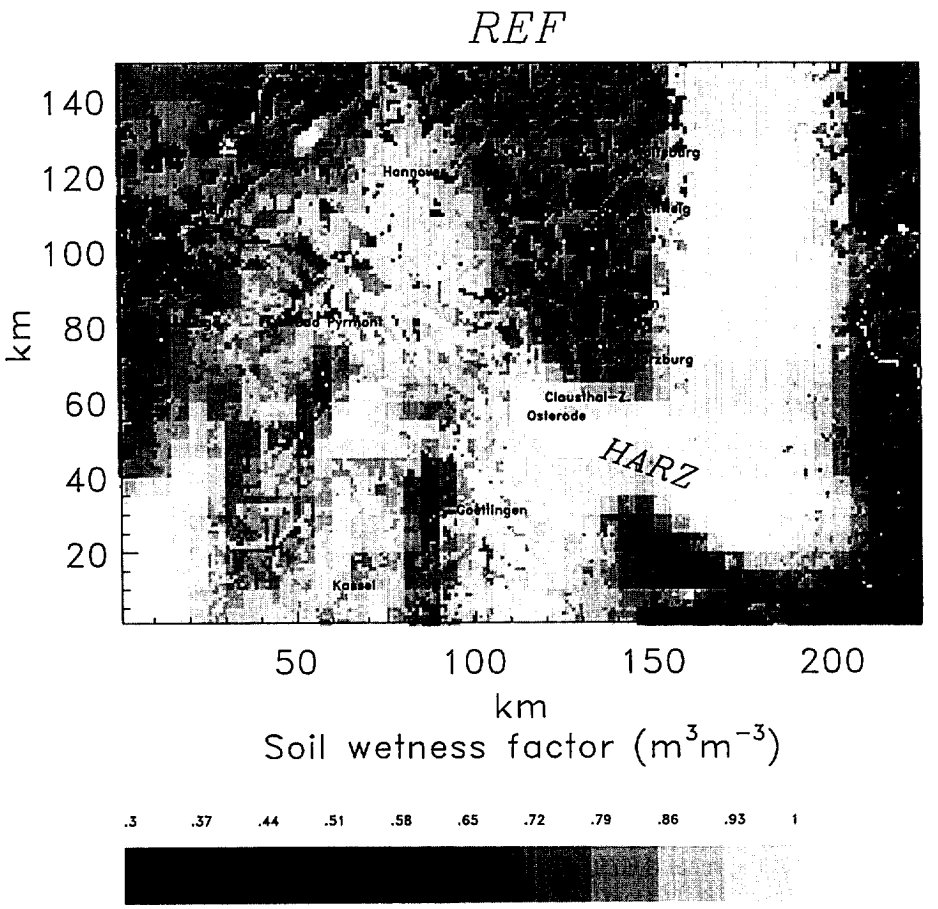

Fig. 6. Soil wetness factor in (m^3 m^{-3}) as predicted by the run without two-way-coupling (REF) for 24 LT.

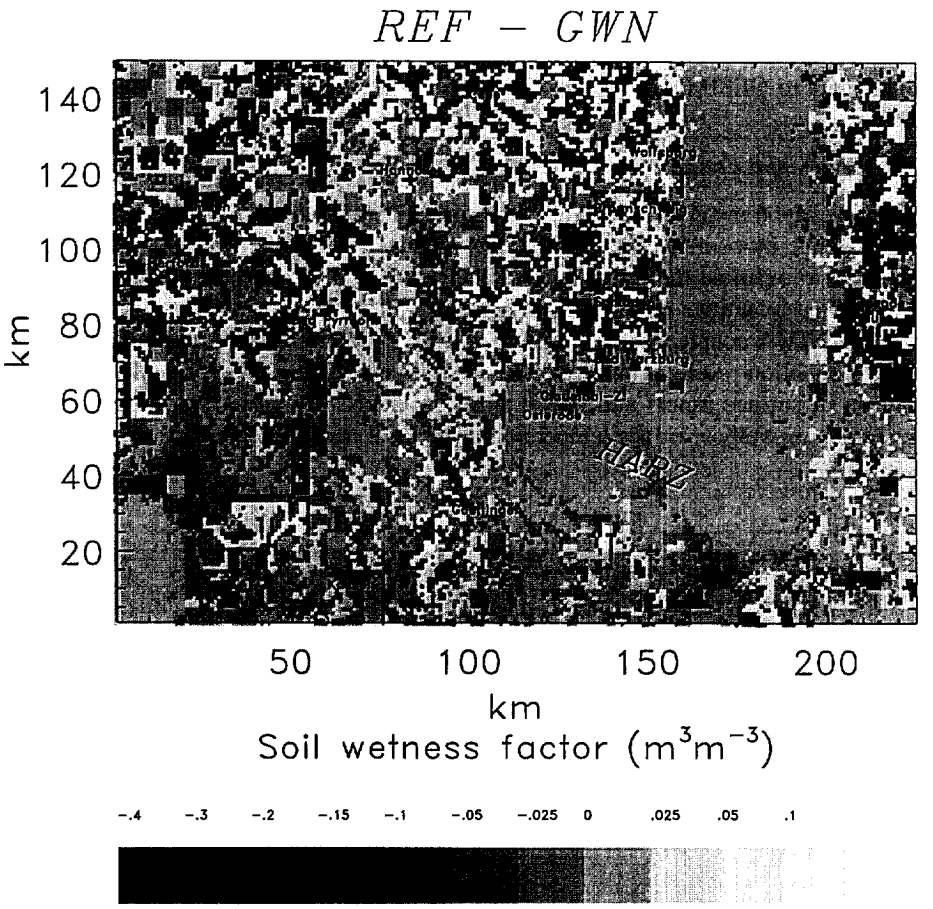

Fig. 7. Differences (REF–GWN) in the soil wetness factors ($m^3\ m^{-3}$) predicted by the run without (REF) and with the two-way-coupling (GWN) for 24 LT.

also results in differences in the fluxes of sensible and latent heat and, hence, Bowen ratio (e.g., Fig. 8) as well as evapotranspiration (e.g., Figs. 9 and 10). This causes secondary differences of soil wetness. Moreover, the thermal regime of the atmospheric boundary layer (ABL) is affected because differences arise by the modified fluxes of sensible and latent heat to the atmosphere. This again influences the cloud and precipitation formation processes. The change of precipitation pattern and intensity (e.g., Figs. 11 and 12) modifies soil wetness again. This is the third component of the change in soil wetness caused by the inclusion of surface runoff and lateral flows.

Following this cycle, the discussion starts with the differences of soil wetness. If not mentioned otherwise comparisons are carried out for the catchment, i.e., the region common to both the models indicated by the thick line in Fig. 1. Note that due to the complex non-linear interactions of the processes involved in the water cycle, it is sometimes unavoidable to mention a phenomenon before its occurrence was explained.

5. Results and discussion

The differences in most of the quantities predicted by the two simulations are greater during the daytime than during the nighttime due to the strong interrelation between the atmospheric water cycle and the energy budget. Nevertheless, the relative differences accumulate with increasing simulation time.

5.1. Soil wetness distribution

As already pointed out, the neglecting of lateral soil water flows and surface runoff usually applied in meteorological models (e.g., Pielke, 1984; Müller et al., 1995) means that the water cycle is not closed. Consequently, if precipitation occurs and the soil becomes saturated, all excess water will get lost and will diminish from the water cycle. This is the case for REF. In GWN, however, water will run off to lower elevated subgrid cells if the soil is saturated. Therefore, integrated over the model domain the soil would contain more water in GWN than in REF if the contributions of the other sinks and sources of water were identical in both the runs.

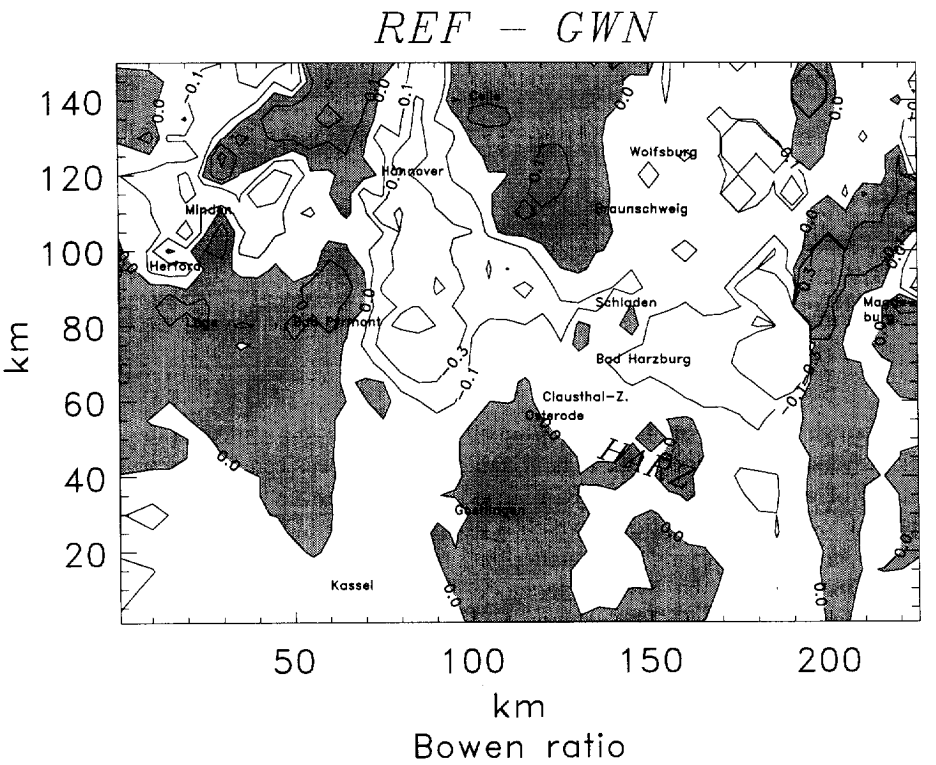

Fig. 8. Differences of Bowen-ratios (REF–GWN) for 12 LT. Grey shaded areas denote positive differences, i.e., REF provides the greater values.

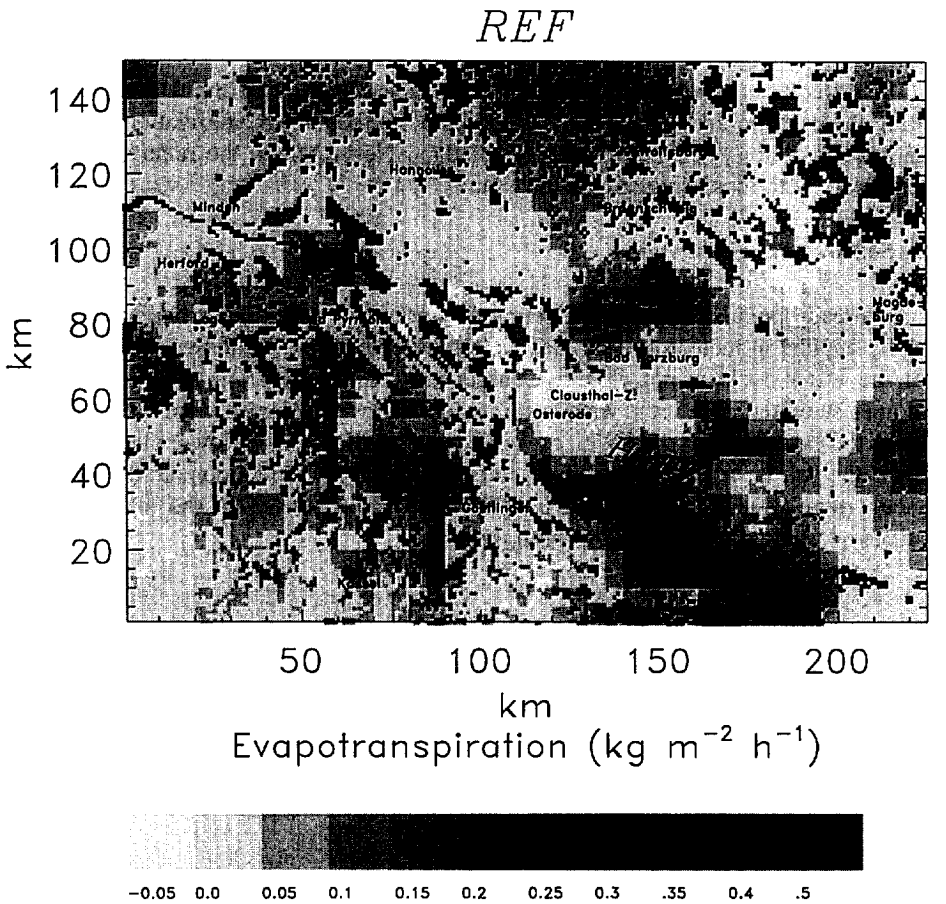

Fig. 9. Evapotranspiration (kg m^{-2} h^{-1}) as predicted by the run without two-way-coupling (REF) for 12 LT.

Although in GWN, on the model domain average, the soil is moister (e.g., Fig. 7), the sinks (evapotranspiration; e.g., Figs. 9 and 10) and sources (precipitation; e.g., Figs. 11 and 12) of water are less than in REF. This clearly evidences that the practice to neglect surface runoff and lateral flows, which is usually applied in meteorological models, may yield to an artificial drying of the underlying surface and a reduced moisture availability.

The inclusion of the hydrologic model leads to a smoothing of the soil wetness distribution in areas with low or none precipitation, for instance, in the region between Hannover, Celle, Wolfsburg and Bad Harzburg. The lateral flow and the changes of soil wetness are the greatest at the boundaries of the model domain of NASMO (e.g., Fig. 7) where in the hours before intense precipitation was predicted by GESIMA (e.g., Figs. 11 and 12).

The contribution of lateral in- and outflow to the change of soil wetness is only about some percent within an hour in our case study. Of course, the changes of the

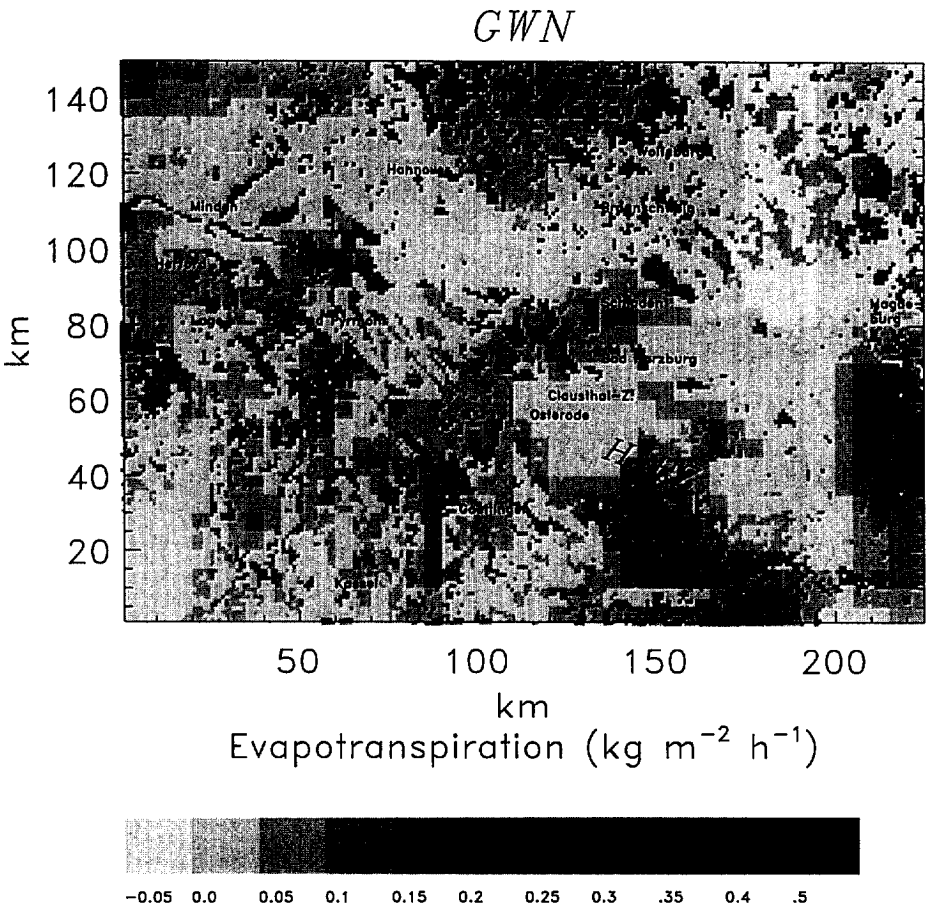

Fig. 10. As Fig. 9 but for the simulation with two-way-coupling (GWN).

evapotranspiration (Figs. 9 and 10), the precipitation pattern and intensity (Figs. 11 and 12), which result as a response to the change of soil moisture, again affect soil wetness and increase the differences between REF and GWN with increasing simulation time.

In the higher elevated areas, a slight drying effect and in the valleys a slight shift towards a wetting can be detected (Fig. 7; e.g., area around Schladen, south of Osterode). Note that in GWN in the water meadows of the river Elbe near Magdeburg the increase of soil moisture is caused by dew.

Comparison of the relationship between soil wetness and elevation after 24 h of simulation evidences that in the higher elevated areas of the catchment soil wetness decreases after a precipitation event (Fig. 13). On the contrary, in the lower elevated areas, where no precipitation fell within the last hour, soil wetness may slightly increase, provided that evapotranspiration is small. If in both the simulations at a location precipitation falls during the last hour, the differences of soil wetness will be small.

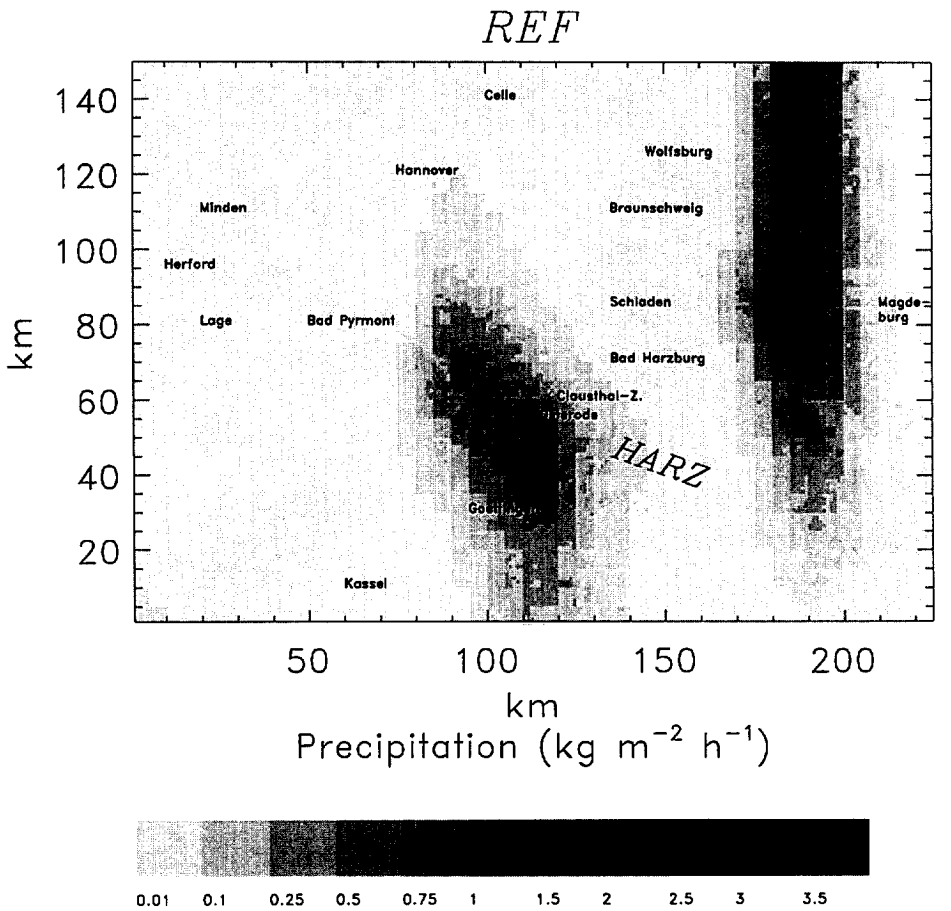

Fig. 11. Precipitation (kg m^{-2} h^{-1}) as predicted by the simulation without two-way-coupling (REF) for 12 LT.

In REF, the elevation–soil wetness relationship results from the increase of precipitation and the decrease of evapotranspiration with increasing height. Additionally, to these effects in GWN surface runoff and lateral flows affect the elevation–soil wetness relationship. As pointed out before, the coupling tends to smooth the discrepancies of soil wetness between valleys and hills (e.g., Figs. 13 and 14).

Altogether, the comparison of the results obtained by the two simulations substantiate that the coupling achieves that the valleys get moister and that the mountain ridges get drier. Hence, in the meteorological model, the two-way-coupling improves the prediction of soil moisture with respect to a more realistic soil wetness elevation relationship.

Note that the differences of soil wetness occurring outside the catchment result from differences in the variables of state of the overlying atmosphere. These differences of advected air temperature and humidity (e.g., Figs. 15 and 16) result in different water and energy fluxes finally leading to these slight differences of soil wetness.

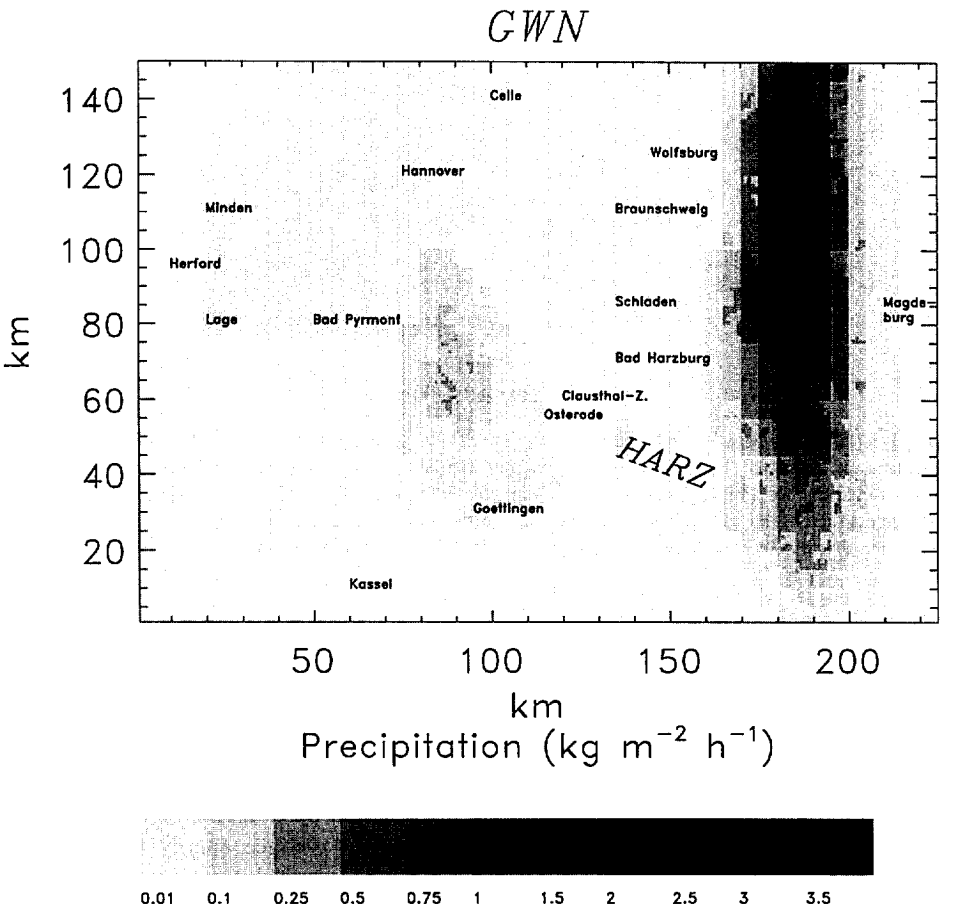

Fig. 12. As Fig. 11 but for the simulation with two-way-coupling (GWN).

5.2. *Energy and water fluxes*

In general, net radiation, soil heat fluxes and the fluxes of sensible and latent heat hardly differ outside the catchment. The inclusion of the coupling leads to smoother distributions of all fluxes as compared with those obtained by the reference run. The fluxes of latent heat react the most sensitive to the coupling, followed by those of sensible heat. Net radiation seems to be the less sensitive component of the energy budget to the changes of soil wetness.

In the catchment, the net radiation predicted by GWN decreases as compared with REF due to the changes of cloud optical properties (the liquid water path decreases). These discrepancies of the predicted energy input on their turn again conduce to differences in latent, sensible and soil heat fluxes. Since in GWN, the insolation is slightly greater due to thinner cloudiness, at some locations outside the catchment the

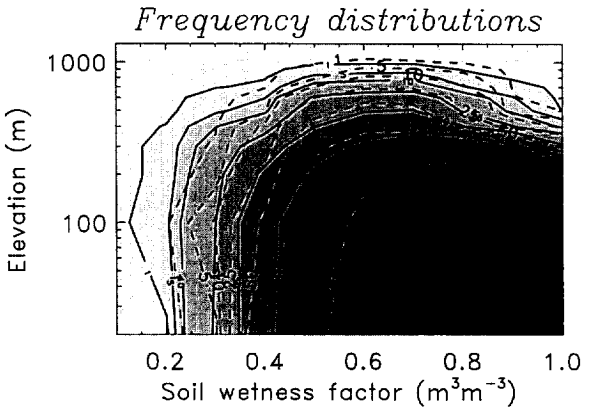

Fig. 13. Relationship between soil wetness factor ($m^3\ m^{-3}$) and subgrid cell surface elevation (m) within the catchment as predicted by the simulation without (REF, grey levels) and (GWN, dashed lines) with two-way-coupling for 24 LT. The contour lines stand for the number of occurrence of subgrid cells with such a soil wetness factor–elevation relationship counted over the entire simulation time using hourly data. Here, only results of subgrid cells that received no precipitation within the last hour are shown.

surface may heat more strongly than in REF during the daytime. This leads to slightly higher soil heat fluxes for GWN than for REF during the daytime. On the contrary, at those locations within the catchment, for which the soil wetness of GWN slightly increased, soil heat fluxes decrease (up to 50 W m^{-2} at noon) as compared with REF. This results in slightly warmer surface temperatures of the vegetated and wetter areas of GWN as compared with REF.

The atmospheric energy and water cycles are coupled by evapotranspiration and the respective latent heat fluxes. The key role of the land surface energy budget is the partitioning of available energy between the latent and sensible heat fluxes which may be characterized by the Bowen ratio, $B = H/L_v E$. Due to our modeling strategy,

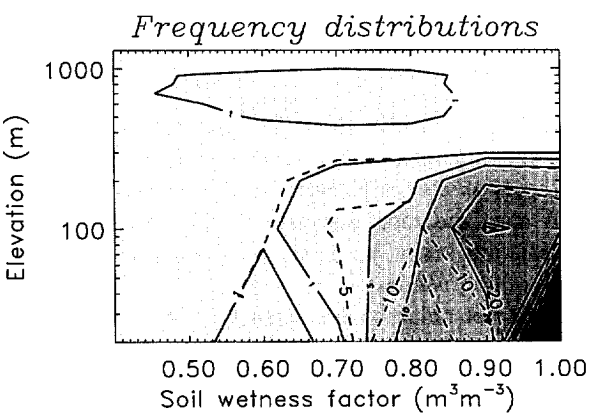

Fig. 14. As Fig. 13 but for those subgrid cells that received precipitation in the last hour.

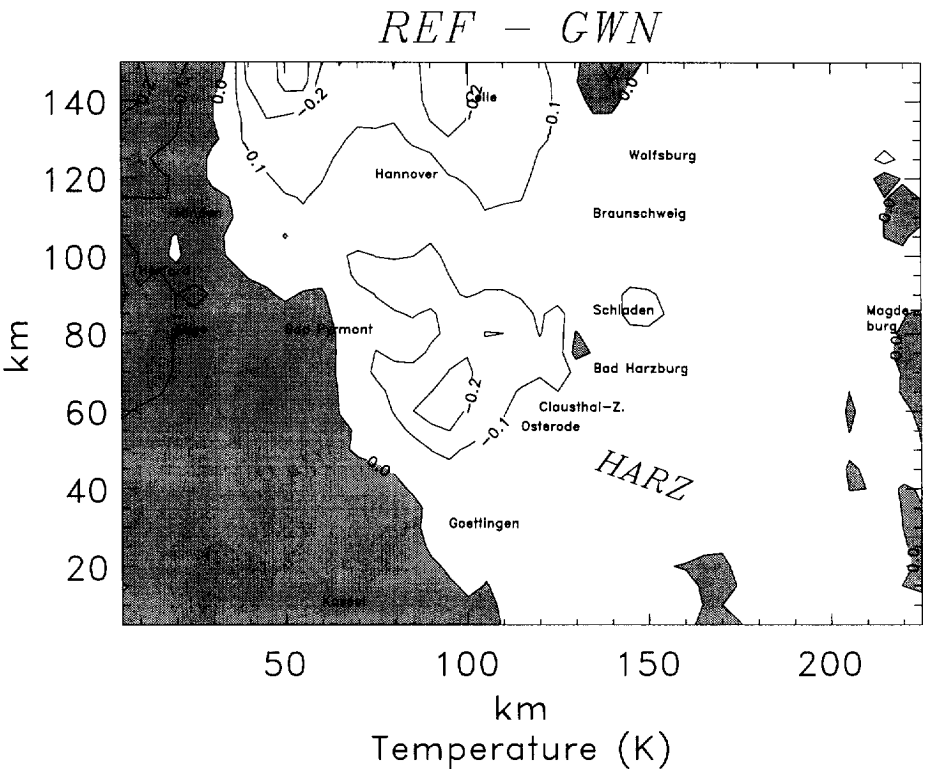

Fig. 15. As Fig. 8 but for temperature (K) in 10 m above ground for 12 LT.

differences of the Bowen ratio (Fig. 8) are primarily caused by the changed soil wetness. Further, differences may result from the modified surface and air temperatures (e.g., Fig. 15).

Despite on average the soil is moister in GWN, the basin averaged Bowen ratio shifts towards higher values relative to REF (see also Fig. 8). Closer examination shows that, on average, the sensible heat fluxes are slightly increased in GWN.

The modification of the latent heat fluxes is more complicated than that of the sensible heat fluxes. For low latent heat fluxes (< 100 W m^{-2}) GWN usually provides increased (up to 50 W m^{-2} at noon) values, while for high latent heat fluxes (> 200 W m^{-2}), it provides lower (up to 30 W m^{-2} at noon) values, i.e., the variability of the latent heat fluxes is lower in GWN than in REF (Figs. 9 and 10). This leads to a slightly extended distribution of evapotranspiration rates between 0.05 to 0.14 kg m^{-2} h^{-1} in GWN as compared with REF (e.g., Figs. 9 and 10; north of the line Kassel, Göttingen, Osterode, Bad Harzburg). On the contrary, the areas providing evapotranspiration rates of more than 0.28 kg m^{-2} h^{-1} decrease as compared with REF (e.g., Figs. 9 and 10; south of the Harz).

There are several reasons. First, if no precipitation falls, greater latent heat fluxes will tend to occur in flat terrain at low elevation above sea level (e.g., Figs. 9 and 10; area

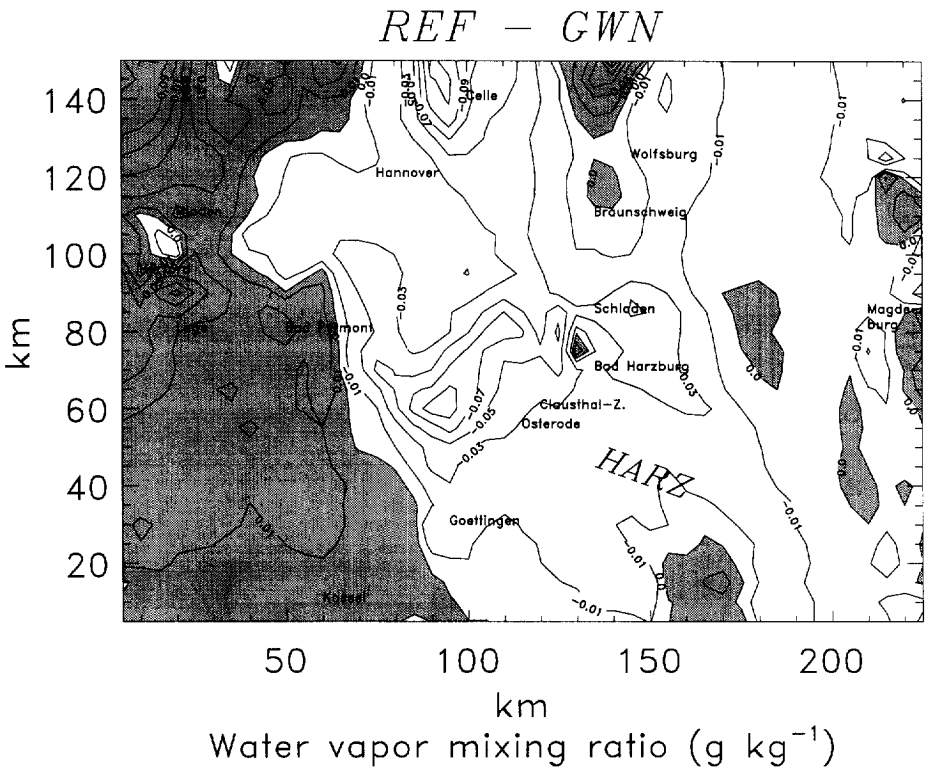

Fig. 16. As Fig. 15 but for humidity (g kg^{-1}).

between Celle, Wolfsburg and Braunschweig) because these areas are often warmer than the mountainous terrain. Although in REF, the valleys are drier (Figs. 6 and 7), they evapotranspirate at higher rates than in GWN, because the slightly higher humidity of the air in GWN (see, e.g., Fig. 16) means a locally lower water vapor deficit.

Second, as mentioned before, due to the inclusion of lateral water flow and surface runoff, soil wetness slightly increases in lower elevated terrain where no precipitation occurred (Fig. 13). This leads to a greater moisture supply to the atmosphere of GWN in areas for which only low evapotranspiration rates were achieved by REF (e.g., Figs. 9 and 10; west of Schladen, east of Hannover).

Third, low latent heat fluxes, however, are often associated with areas of precipitation. Here, the water vapor deficit is low due to evaporation of raindrops. The related evaporative cooling decreases the air temperature. This again decreases the water vapor deficit and, hence, the evapo(transpi)ration from the surface. Since water has to be extracted from the soil against capillary and adhesive forces before it can evaporate, the contribution of rainwater evaporation to the reduction of the water vapor deficit of the near surface layer can be greater than that of evaporation. In GWN, as will be discussed later, the rainwater mixing ratios are often slightly lower than in REF. Therefore, in

GWN at some locations, the evaporation of soil water is slightly increased as compared to REF (e.g., Figs. 9–12; west of Osterode).

5.3. Air temperature and humidity distribution

The temperature and moisture states in the system Earth–atmosphere evolve by fluxes which themselves depend on those states. The resultant non-linear dynamical system has modes of variability that depend on the interactions of the energy and water budget (Entekhabi and Brubaker, 1995). As expected, the predicted air temperatures and humidity hardly differ in the upper troposphere. In the ABL and the mid-troposphere locally, the grid cell by grid cell differences grow due to differences in phase transition processes and vertical motions. Nevertheless, in the ABL, the differences of predicted air temperature and humidity rise by approaching the Earth's surface.

Like for soil wetness and the surface fluxes, the greatest differences between the predictions of humidity and air temperature, respectively, occur in the ABL above the catchment (e.g., Figs. 15 and 16). Here, on the average the air temperatures are slightly warmer (about 0.2 K) in GWN than in REF during the daytime (e.g., Fig. 15). This is mainly caused by the stronger sensible heat fluxes, the slightly increased insolation resulting from the slightly thinner cloudiness (see Section 5.4), and the slightly warmer surface temperatures within the catchment in GWN than in REF.

The predicted distribution of humidity changes in a more complicated way than that of temperature. North west of Hannover, for instance, humidity slightly decreases due to the lower evapotranspiration of GWN as compared with REF (e.g., Fig. 16). In the other regions of the catchment, humidity increases in GWN as compared to REF. The predicted water vapor distributions more strongly differ in flat terrain and in the regions, for which precipitation is predicted in both the runs, than in mountainous terrain. In flat terrain, the increase of water vapor may be attributed to the moister soil and, hence, slightly enhanced evapotranspiration of GWN. In the other regions of the catchment, the slightly warmer air and the differences in phase transition processes among others contribute to the grown water vapor.

5.4. Clouds and precipitation

In the mid-troposphere, the predicted distributions of water substances slightly differ from differences in phase transition processes, vertical motions, turbulence or radiative cooling. These differences vanish with increasing height. In the ABL, however, the slightly warmer air temperatures of GWN (see also Fig. 15) lead to a lower relative humidity and slightly lower mixing ratios of cloud water, rainwater, ice and graupel as compared to REF (up to 0.2 g kg^{-1}). Since a mass-weighted (according to the ice and cloud water already present) saturation adjustment scheme is applied for the temperature range (-35°C and 0°C) of coexistence of frozen and supercooled water (Mölders et al., 1995, 1997), the mass-weighted saturation mixing ratios are often higher in GWN than in REF. Hence, the onset of condensation and deposition is shifted towards higher relative humidity (with respect to water) which means that in the warmer atmosphere of GWN less cloud water and ice is formed than in REF. In addition, in the cloud

parameterization scheme, the partitioning of the excess water vapor between cloud water and ice depends on the degree of supercooling (Mölders et al., 1995, 1997). Consequently, the formation of ice is slightly favored in REF which again lowers the mass-weighted saturation mixing ratios of REF as compared to GWN.

Only, in those lower elevated areas with increased soil wetness and evapotranspiration where, moreover, no precipitation fell in the last hours, or so, the cloud and precipitating particle mixing ratios are slightly greater (about 0.05 g kg^{-1}) in GWN than in REF during the daytime. In the region of the common model domain, the mixing ratios of the cloud and precipitating particles differ the strongest, especially, in the areas around Schladen, Bad Harzburg and Göttingen as well as south of Hannover. Here, lateral flows, runoff and the differences of evapotranspiration are the greatest, too.

In GWN, the decrease of the mixing ratios of the cloud and precipitating particles goes along with a less intense precipitation and a horizontally less extended precipitation distribution as compared to REF (e.g., Figs. 11 and 12). These differences again affect soil wetness distribution, evapotranspiration (e.g., Figs. 9 and 10), cloud and precipitation formation. Therefore, the relative differences of water cycle relevant quantities grow with increasing simulation time.

6. Summary and conclusions

A module to couple a meteorological and a runoff model was presented. By explicitly breaking down the grid cells of the meteorological model, the spatial location of each subgrid flux is known (Fig. 3). Hence, evapotranspiration, precipitation and soil wetness can be provided for gridded hydrologic models in a much finer resolution than that of the meteorological model. The lateral differences of inflow and outflow provided by the hydrologic model, which is driven by the meteorological model, serve to consider surface runoff and lateral flows in the meteorological model. Implementation of the module in meteorological models requires landuse, soil and topographical data in the resolution of the desired subgrid.

Simulations with and without a two-way-coupling of the meteorological and the hydrologic model were carried out to test the effect of a two-way-coupling on the predicted local weather. The results substantiate that there is a visible impact of surface hydrology on cloud and precipitation formation. This indicates that further affords are required on a better consideration of the land phase of the water cycle in weather forecasting, climate as well as in chemical transport modeling.

There is still a lot of work to be done in the future. First of all, some inconsistencies between the models have to be removed. For instance, the effect of soil temperature on runoff has to be included in NASMO. Secondly, improvements for the application on a wider spectrum of synoptic situations are required. For example, at the moment all subgrid cells within a grid cell will receive a height-dependent amount of precipitation if the cloud module predicts precipitation. Such a parameterization only works for stratiform precipitation events. Therefore, a parameterization that allows to heterogenize convective precipitation has to be developed. Here, semi-empirical approaches wherein subgrid-scale precipitation is related with cloud base height and upwind landuse conditions might be conceivable.

Evaluation of the explicit subgrid scheme as well as of the two-way-coupling by means of measured data must be postponed until complete suitable data sets are available. Here, the uncertainty in the measured data must be at least an order of magnitude lower than the differences between the simulations. This task will hopefully be addressed within the framework of the GEWEX field campaigns.

Acknowledgement

We would like to express our thanks to the Minister of Education, Science, Research and Technology (BMBF) of Germany for the support of this study within the framework of the Water Cycle Project, contract 521-4007-07 VWK01. We are grateful to Th. Beckmann from the Leichtweiß Institut für Wasserbau, Abt. Hydrologie und Wasserwirtschaft of the Technische Universität Braunschweig for performing the simulations with NASMO and for providing the lateral differences of inflow and outflow. Thanks also to K. Friedrich and C. Leicht for digitizing the landuse and topography data. We also wish to thank U. Maniak, A. Ziemann, G. Kramm, K.E. Erdmann, J. Dessens and the two anonymous reviewers for fruitful discussions and helpful comments.

Appendix A. List of symbols

c_i	Heat capacity	J m^{-3} K^{-1}
c_p	Specific heat at constant pressure	J kg^{-1} K^{-1}
f	Soil wetness factor	m^3 m^{-3}
g_s	Canopy conductivity	m s^{-1}
g_1	Maximal evaporative conductivity	m s^{-1}
k_s	Diffusion coefficient	m^2 s^{-1}
q	Specific humidity	kg kg^{-1}
q_s	Specific humidity of saturation	kg kg^{-1}
t	Time	s
u	Wind	m s^{-1}
w_e	Wetness factor	m^3 m^{-3}
w_k	Field capacity	m
z	Terrain elevation/depth of soil	m
z_0	Roughness length	m
C_h	Transfer coefficient for heat	–
C_q	Transfer coefficient for water vapor	–
E	Evapo(transpi)ration	kg m^{-2} s^{-1}
F_j^k	Mean flux in the jth atmospheric grid cell	W m^{-2}
G	Soil heat flux	W m^{-2}
H	Sensible heat flux	W m^{-2}
L	Longwave radiation	W m^{-2}
L_v	Latent heat of condensation	J kg^{-1}
$L_v E$	Latent heat flux	W m^{-2}

N	Number of subgrid cells within a grid cell	–
P	Precipitation	kg m^{-2} s^{-1}
Q	Net radiation	W m^{-2}
R	Difference of lateral in- and outflow	kg m^{-2} s^{-1}
S	Shortwave radiation	W m^{-2}
T	Temperature	K
α	Albedo	–
α_c	Capillarity	kg m^{-3} s^{-1}
β	Switch parameter	–
ε	Emissivity	–
σ	Stephan–Boltzmann constant	W m^{-2} K^{-4}
λ	Soil thermal conductivity	J K^{-1} s^{-1} m^{-1}
ρ	Density of air	kg m^{-3}
ρ_w	Density of water	kg m^{-3}
Θ	Potential temperature	K

References

Deardorff, J.W., 1978. Efficient prediction of ground surface temperature and moisture, with inclusion of a layer of vegetation. J. Geophys. Res. 84C, 1889–1903.

Dingman, S.L., 1994. Physical Hydrology. Macmillan, New York.

Entekhabi, D., Brubaker, K.L., 1995. An analytical approach to modeling land–atmosphere interaction: 2. Stochastic formulation. Water Resour. Res. 31, 633–643.

Eppel, D.P., Kapitza, H., Claussen, M., Jacob, D., Koch, W., Levkov, L., Mengelkamp, H.-T., Werrmann, N., 1995. The non-hydrostatic mesoscale model GESIMA: Part II: Parameterizations and applications. Contr. Atmos. Phys. 68, 15–41.

Giorgi, F., 1990. Simulation of regional climate using a limited area model nested in a general circulation model. J. Clim. 3, 941–963.

Hagemann, S., Dümenil, L., 1996. Development of a parameterization of lateral discharge for the global scale. MPI Report No. 219.

Hupfer, P., Raabe, A., 1994. Meteorological transition between land and sea in the microscale. Met. Z. 3, 100–103.

Johnson, G.L., Hanson, C.L., 1995. Topographic and atmospheric influences on precipitation variability over a mountainous water shed. J. Appl. Meteor. 34, 68–87.

Kapitza, H., Eppel, D.P., 1992. The non-hydrostatic mesoscale model GESIMA: Part I: Dynamical equations and tests. Contr. Atmos. Phys. 65, 129–146.

Kessler, E., 1969. On the distribution and continuity of water substance in atmospheric circulations. Meteor. Monogr. 27, Am. Meteor. Soc. 84.

Kleeberg, H.-B., Øverland, H., 1989. Zur Berechnung des effektiven oder abflußwirksamen Niederschlags. Mitt. Inst. f. Wasserwesen 32, 19–62.

Kramm, G., Dlugi, R., Dollard, G.J., Foken, T., Mölders, N., Müller, H., Seiler, W., Sievering, H., 1995. On the dry deposition of ozone and reactive nitrogen compounds. Atmos. Environ. 29, 3209–3231.

Kuhl, S.C., Miller, J.R., 1992. Seasonal river runoff calculated from a global atmospheric model. Water Resour. Res. 28, 2029–2039.

Leung, L.R., Ghan, S.J., 1995. A subgrid parameterization of orographic precipitation. Theor. Appl. Climatol. 52, 95–118.

Liston, G.E., Sud, Y.C., Wood, E.F., 1994. Evaluating GCM land surface hydrology parameterizations by computing river discharges using a runoff routing model: application to the Mississippi Basin. J. Appl. Met. 33, 394–405.

Mahrt, L., Sun, J., 1995. Dependence of exchange coefficients on averaging scale and grid size. Q. J. R. Met. Soc. 121, 1835–1852.

Maniak, U., 1996. Gitterpunktgestütztes Flußgebietsmodell als Abflußmodul eines Wasserhaushalts-bzn. Klimamodells, Zwischenbericht.

Marengo, J.A., Miller, J.R., Russel, G.L., Rosenzweig, C.E., Abramapoulos, F., 1994. Calculations of river-runoff in the GISS GCM: impact of a new land-surface parameterization and runoff routing model on the hydrology of the Amazon river. Clim. Dyn. 10, 349–361.

Miller, J.R., Russel, G.L., Caliri, G., 1994. Continental-scale river flow in climate models. J. Clim. 7, 914–928.

Milly, P.C.D., Dunne, K.A., 1994. Sensitivity of the global water cycle to the water-holding capacity of land. J. Clim. 7, 506–526.

Mölders, N., Laube, M., Kramm, G., 1995. On the parameterization of ice microphysics in a mesoscale α weather forecast model. Atmos. Res. 38, 207–235.

Mölders, N., Raabe, A., Tetzlaff, G., 1996. A comparison of two strategies on land surface heterogeneity used in a mesoscale β meteorological model. Tellus 48A, 733–749.

Mölders, N., Kramm, G., Laube, M., Raabe, A., 1997. On the influence of bulk-parameterization schemes of cloud microphysics on the predicted water-cycle relevant quantities: a case study. Met. Z. 6, 21–32.

Müller, E., Foken, T., Heise, E., Majewski, D., 1995. LITFASS: A nucleus for a BALTEX field experiment. DWD Arbeitsergebnisse No. 33.

Pielke, R.A., 1984. Mesoscale Meteorological Modeling. Academic Press, London.

Pleiss, H., 1977. Der Kreislauf des Wassers in der Natur, VEB G. Fischer Verlag, Jena.

Raabe, A., 1983. On the relation between the drag coefficient and fetch above the sea in the case of off shore wind in the near-shore zone. Z. Meteor. 6, 363–367.

Raabe, A., 1991. Die Höhe der internen Grenzschicht. Z. Meteor. 41, 251–261.

Sausen, R., Schubert, S., Dümenil, L., 1994. A model of the river runoff for use in coupled atmosphere–ocean models. J. Hydrol. 155, 337–352.

Seth, A., Giorgi, F., Dickinson, R.E., 1994. Simulating fluxes from heterogeneous land surfaces: explicit subgrid method employing the biosphere–atmosphere transfer scheme (BATS). J. Geophys. Res. 99D, 18651–18667.

von Storch, H., Zorita, E., Cubasch, U., 1993. Downscaling of global climate change estimates to regional scales: an application to Iberian rainfall in wintertime. J. Clim. 6, 1161–1171.

Tetzlaff, G., Mölders, N., 1997. Beurteilung der Modellierbarkeit des flächenbezogenen Eintrags von Spurenstoffen durch Deposition. Wiss. Mitt. Inst. f. Meteor., Inst. f. Troposphären-forschung 6, 47.

Wilson, M.F., Henderson-Sellers, A., Dickinson, R.E., Kennedy, P.J., 1987. Sensitivity of the biosphere–atmosphere transfer scheme (BATS) to the inclusion of variable soil characteristics. J. Clim. Appl. Met. 26, 341–362.